CHALMERS

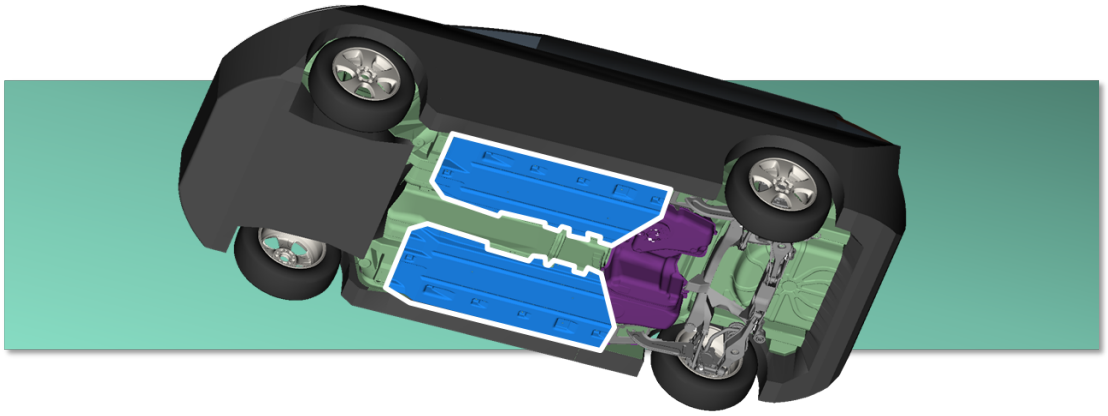

# Fluid structure interaction analysis on the aerodynamic performance of underbody panels

*Master's thesis in fluid and solid mechanics*

JARI KESTI
SIMON OLSSON

Department of Applied Mechanics
*Division of Fluid Dynamics*
Chalmers University of Technology
Göteborg, Sweden 2014
Master's Thesis 2014:68

MASTER'S THESIS IN FLUID AND SOLID MECHANICS

# Fluid structure interaction analysis on the aerodynamic performance of underbody panels

JARI KESTI
SIMON OLSSON

Department of Applied Mechanics
*Division of Fluid Dynamics*
CHALMERS UNIVERSITY OF TECHNOLOGY
Göteborg, Sweden 2014

Fluid structure interaction analysis on the aerodynamic performance
of underbody panels
JARI KESTI
SIMON OLSSON



Master's thesis 2014:68
ISSN 1652-8557
Department of Applied Mechanics
Division of Fluid Dynamics
Chalmers University of Technology
SE-412 96 Göteborg
Sweden
Telephone: +46 (0)31-772 1000

Cover:
The car geometry used in the project showing the location of the underbody panels underneath the car.

Chalmers Reproservice
Göteborg, Sweden 2014

Fluid structure interaction analysis on the aerodynamic performance
of underbody panels
Master's thesis in fluid and solid mechanics
JARI KESTI
SIMON OLSSON
Department of Applied Mechanics
Division of Fluid Dynamics
Chalmers University of Technology

**Abstract**

Underbody panels cover the rough surface under the car in order to reduce turbulence. They have a weak structure and might deform when subjected to the surrounding high speed flow. It is important to consider this deformation and to analyse how it might affect the performance of the underbody panels, both aerodynamic (drag and lift forces) and structural (stresses).

In this thesis, analyses on these underbody panels are perfomed using a method called Fluid Structure Interaction (FSI). In FSI the fluid and structure are treated as a coupled system. A FSI script-based system for steady analysis has been created between the fluid solver Ansys Fluent and the structural solver MSC Nastran. Results from simulations have been validated with the already available FSI software System Coupling in Ansys Workbench.

The results showed that the deformations of the underbody panels were small. These small deformations had no major impact on the drag, lift or stresses in the panels. The maximum deformations of the underbody panels were in the range between 0.2-0.3 mm, with a maximum stress of about 3.0 MPa.

Evaluation of the FSI method used in this project, showed that a deforming mesh is the most important and challenging area. The method for mesh movement in this project was not robust enough. Therefore another method for moving the mesh have to be implemented in the future. The small deformations of the underbody panels, from steady state simulations, indicate that it is faster and easier to *only* consider the pressure from the high speed flow. For future analyses of underbody panels and other systems with small deformations, it could be relevant to consider time-dependent simulations. Oscillations in systems, noise and failure due to vibrations are important to evaluate.

**Keywords:** Fluid Structure Interaction, FSI, Underbody Panels, Aerodynamics, Partitioned Approach, Automotive Industry

## Acknowledgements

We would like to thank our supervisors at CEVT, Jesper Marklund and Andreas Blixt for all the guidance and support given to us during the Master's thesis project. We would also like to thank Ansys Sweden for their interest and software support during the setup of Ansys Workbench. A special thank you to Tobias Berg at Ansys Sweden for his technical support and useful input during the simulation process. Furthermore we would like to thank our examiner Prof. Lars Davidson at Chalmers for his help and advice during the project. Lastly, we send our gratitude to all employees at CEVT that contributed by sharing their knowledge and insights to make this project successful.

Jari Kesti & Simon Olsson, Göteborg October 29, 2014

# Contents

# 1

# Introduction

This Master's thesis project was carried out at Chalmers University of Technology, developed for China-Euro Vehicle Technology (CEVT) during 2014. It includes a fluid structure interaction analysis of underbody panels for future C-segment cars. It also covers an evaluation of a fluid structure interaction method that can be applied when solving aerodynamic problems in the vehicle industry.

## 1.1 Background

In the beginning of 2013, Geely Group created China-Euro Vehicle Technology AB (CEVT), which is an engineering and development company for future C-segment cars. Like in so many other industries today, *computer-aided engineering* (CAE) plays an important role in research and product development. *Computational fluid dynamics* (CFD) and *finite element analysis* (FEA) are both part of CAE. When a system includes both a liquid and a solid phase that are strongly coupled, analysis requires CFD and FEA to be carried out simultaneously in what is called *fluid structure interaction* (FSI).

In aerodynamics for example, the car is generally treated as a rigid body. This is a good enough approximation for most parts of the vehicle. However, in some areas where the flow speed is high and the structure is weak, there might be deformations that cannot be neglected. These deformations may have an impact on the air flow and affect the accuracy of the results from drag and lift force simulations.

One part of the vehicle where this might occur is the underbody panels. These panels cover the rough surface underneath the car to reduce turbulence. They are designed to be lightweight and cover a large surface area. This may result in a weak structure that is affected by large aerodynamic forces under the car. The panels deform and it is of great importance to investigate the impact the deformations have on the vehicle aerodynamic performance.

## 1.2 Aim

The underbody panels are used in passenger vehicles mainly to reduce turbulence formed by the rough surface under the car. Because of the need to reduce weight and fuel consumption in the automotive industry, the underbody panels are made as light and thin as possible. If their weak structure deforms, the effects on drag, lift and stress distribution on the panels could be large enough that the deformations can no longer be considered negligible.

The purpose of this thesis work is to find how these aerodynamic properties of deformable underbody panels change during fluid structure interaction. At the same time develop and evaluate a FSI method that should be fast and robust for the daily projects in automotive CFD applications.

To achieve the aim of the project, the following research questions are answered:

- For an undeformed underbody panel, what are the drag and lift coefficients ($C_d$ and $C_l$)?
- What deformations and stress distribution does the flow field around an underbody panel give rise to?
- What is the combined impact of flow field and displacement on the stress distribution and drag/lift coefficient?

## 1.3 Scope and limitations

The scope of this project is to perform FSI simulations where the flow past the vehicle is analysed in conjunction with structural simulations of the underbody panels underneath the vehicle. However, no consideration is taken to material durability or crack growth. The evaluated FSI method is script based and makes use of existing commercial software available at CEVT. Validation of results are performed through existing commercial FSI software, Ansys Workbench.

Studies are only done on high-speed (top speed) flow where the deformations are large enough to be relevant. The vehicle is considered to have a rigid suspension with no initial dynamic loads. Simulations are only performed assuming a flat and smooth ground surface. The project is limited to a time-independent problem so that only static structural and steady state flow simulation are analysed.

## 1.4 Problem formulation

For the flow under the car to be well represented during FSI simulation, a full model of the exterior of a car is used. The model is placed in a wind tunnel-like fluid domain. Because of asymmetry in the model, the entire car is used. Boundary conditions are set to emulate the car driving at top speed. See figure 1.1 for a schematic view of the domain.

The inlet velocity $U$ is 200 km/h or 55 m/s. The road is moving with the same speed $U$. This corresponds to a wheel rotational speed of 166.7 rad/s. This is implemented using a *moving wall* boundary condition. The road moves in the x-direction and the wheels rotate around their centre axis.

A symmetry condition is used on the sides as well as the top of the domain. The gauge pressure at the outlet is set to 0 Pa relative to the operating condition at 1 atm. The air flow is considered time-independent (steady state) and turbulence effects are taken into account by the *realisable* $k$-$\epsilon$ turbulence model.

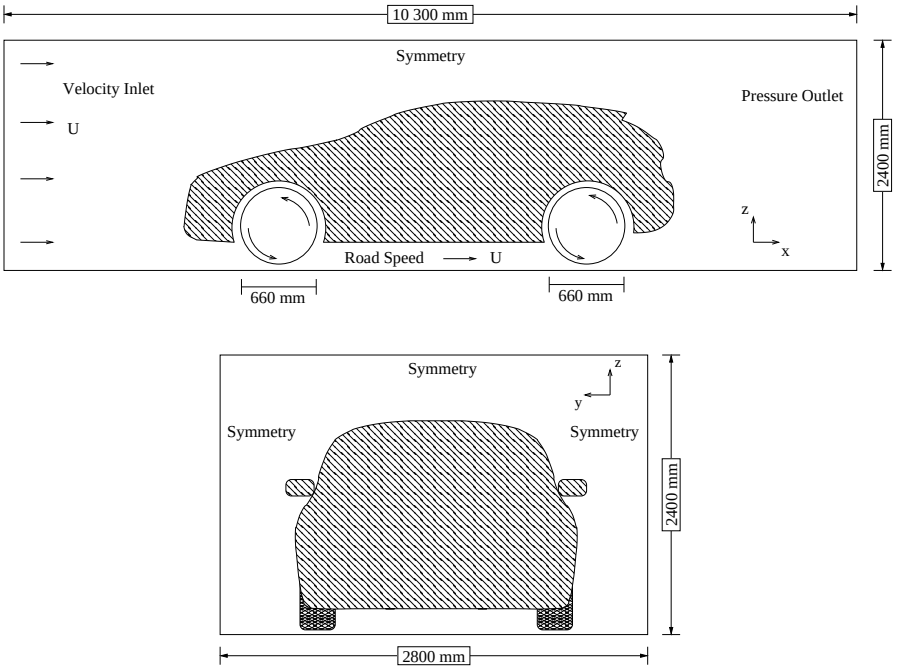


**Figure 1.1:** Schematic side view and front view of the car placed in the fluid domain.

For structural simulation, the underbody panels are assumed to be made of polypropylene with 30 percent glass fiber (PP-GF30). The material is considered to be isotropic with mechanical properties that can be seen in table 1.1. On all holes on the underbody panels, a *fixed support* boundary condition is applied. This is where the panels are attached to the car.

**Table 1.1:** Material properties of the underbody panels.

| Polypropylene (PP-GF30) | |
|---:|:---:|
| Density | 1.140 g/cm$^3$ |
| Young's modulus | 3.0 GPa |
| Poisson ratio | 0.3 |

## 1.5 Thesis outline

Following this introduction, the theory behind fluid structure interaction is covered. One of the ways to classify the amount of interaction (the degree of coupling) between the fluid and structural system is shown. Governing equations in both fluid and structural analysis is then presented, followed by a brief section covering the coupling conditions between the two systems.

The methodology is explained, covering all steps implemented for the fluid structure interaction. Results from simulations and analyses are presented, before a discussion regarding the results. The fluid structure interaction method is evaluated and some major and minor improvements are discussed.

Lastly the work is summarised and final conclusions are drawn.

# 2

# Theory

## 2.1 Fluid structure interaction

Fluid structure interaction (FSI) is a classification of problems where there exist a strong dependency between solid objects and fluids. These systems can be natural or man-made and can be found in many fields of science between engineering and medicine.

Common for all applications in FSI is that there exist an *interface surface* between the solid and the fluid domain. At this interface surface, both the governing equations and the boundary conditions from the fluid and solid domain must be satisfied simultaneously. To close the system of equations at the fluid structure interface, a set of coupling boundary conditions are introduced. These types of coupling conditions can be categorised into a *kinematic* and a *traction (dynamic)* condition. The kinematic condition defines the motion and the traction condition satisfies the stress/force balance [1, 2, 3, 4, 5].

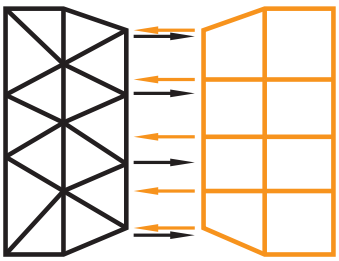

**Figure 2.1:** A non-conformal mesh.

The numerical discretisation is also of great importance in FSI, especially at the interface surface. One option is to discretise the fluid and the solid systems together, which can be solved using a so-called *monolithic approach* (also called *fully coupled*). The governing equations of the fluid and solid are solved together. This requires a conformal

mesh with matching nodal positions between the fluid and solid meshes. This system is very robust but requires a fully integrated FSI solver.

Another option is the *partitioned approach* (also called *staggered*). The fluid and the solid phase can be solved using separate solvers, in sequential order. The mesh can therefore be non-conformal, which means that nodal positions do *not* need to be matched, see figure 2.1. This is a very fast and efficient way of solving FSI problems, even though convergence problems are more frequent than for a monolithic approach [1, 2, 3, 6, 7, 8].

An overview of the two solving precedures in FSI can be seen in figure 2.2.

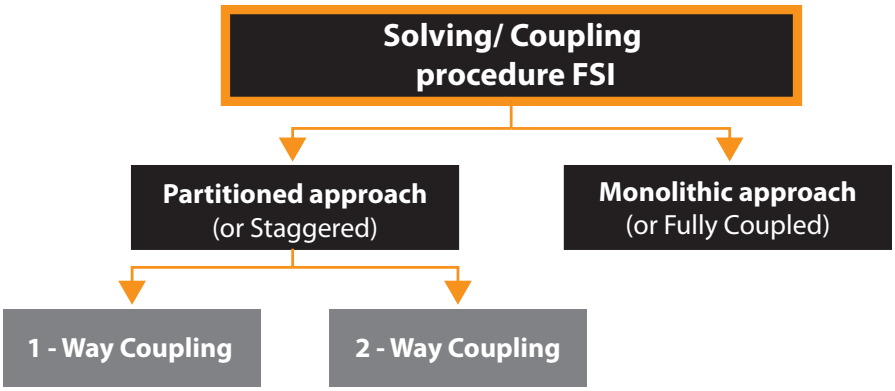


**Figure 2.2:** Solving procedures in FSI.

From now on only the partitioned approach is considered. This solution method can be further divided into a *one-way* and a *two-way* coupling procedure [3].

### 2.1.1 One-way and two-way coupling

In partitioned FSI one-way coupling, transfer quantities are sent from one domain to the other, but not in the opposite direction. For example, the fluid pressure on the structure might be transferred to the solid solver, but the solid displacement is not transferred back to the fluid solver. This is often a good enough approximation for systems where there are no large deformations.

In two-way coupling, the solver data is always transferred both ways at the fluid structure interface. For example, the fluid pressure is transferred to the solid solver. Using the pressure from the fluid as an external load, the resulting displacement of the structure is transferred back to the fluid solver. This procedure of transferring data between the systems continues in an iterative process [3, 9].

## 2.2 Governing equations fluid

The governing equations of fluid flow comprises the conservation of mass and momentum[1]. The continuity equation (conservation of mass) can be expressed as [10]:

$$\frac{d\rho}{dt} + \rho\frac{\partial v_i}{\partial x_i} = 0 \tag{2.1}$$

A common rule is that for airflows with Mach number less than 0.3, it is acceptable to assume air to be incompressible. For incompressible fluid the continuity equation then reduces to [2]:

$$\frac{\partial v_i}{\partial x_i} = 0 \tag{2.2}$$

The balance equation for linear momentum reads [10]:

$$\rho\frac{dv_i}{dt} = \frac{\partial \sigma_{ji}}{\partial x_j} + \rho f_i \tag{2.3}$$

where $\sigma_{ji}$ is the stress tensor and $f_i$ represent external forces per unit mass.

From the momentum equation 2.3, assuming the constitutive equations of a Newtonian viscous fluid and incompressible flow, the Navier-Stokes equationsns can be constructed. Neglecting body forces ($f_i$), these equations read:

$$\rho\frac{dv_i}{dt} = -\frac{\partial p}{\partial x_i} + \frac{\partial \tau_{ji}}{\partial x_j} = -\frac{\partial p}{\partial x_i} + \mu\frac{\partial^2 v_i}{\partial x_j \partial x_j} \tag{2.4}$$

The Navier-Stokes equations are used to solve the flow field in the domain. For a more detailed derivation of the equations, see for example [10, 11].

### 2.2.1 Turbulence model

In turbulent flow the instantaneous variables are preferably decomposed into a mean value (time averaged) and a fluctuating value. To simplify the turbulent fluid problem the Navier-Stokes equation are usually time averaged (steady state condition) into Reynolds Averaged Navier-Stokes (RANS) equation. This time averaging creates a new term called the Reynolds stresses ($-\rho\overline{u_i' u_j'}$), which is an approximation that needs to be modelled.

A common turbulence model is the *realisable* $k$-$\epsilon$ model. The term *realisable* means that the model satisfies the two conditions for realisability. The two conditions are that the normal Reynolds stresses should stay positive, and that the Schwarz inequality for the Reynolds stresses should not be violated:

$$\overline{v_i'^2} \geq 0 \text{ for all } i \tag{2.5}$$

[1]For compressible flows and other flows including any form of heat transfer, conservation of energy is added to the governing equations.

$$\frac{\overline{v_i' v_j'}}{\left(\overline{v_i'^2 v_j'^2}\right)^{1/2}} \leq 1 \text{ no summation over } i \text{ and } j, i \neq j \tag{2.6}$$

For details on these conditions, see for example [10, 12].

Assuming incompressibility and no production of $k$ or $\epsilon$ due to bouyancy, the modeled equations for $k$ and $\epsilon$ in the realisable model are:

$$\frac{\partial k}{\partial t} + \bar{u_j}\frac{\partial k}{\partial x_j} = \frac{\partial}{\partial x_j}\left[\left(\nu + \frac{\nu_t}{\sigma_k}\right)\frac{\partial k}{\partial x_j}\right] + 2\nu_t \bar{S}_{ij}\bar{S}_{ij} - \epsilon \tag{2.7}$$

$$\frac{\partial \epsilon}{\partial t} + \bar{u_j}\frac{\partial \epsilon}{\partial x_j} = \frac{\partial}{\partial x_j}\left[\left(\nu + \frac{\nu_t}{\sigma_\epsilon}\right)\frac{\partial \epsilon}{\partial x_j}\right] + \epsilon C_1 S - C_2\frac{\epsilon^2}{k + \sqrt{\nu\epsilon}} \tag{2.8}$$

where $\bar{S}_{ij}$ is the mean strain rate tensor ($\bar{S}_{ij} = \frac{1}{2}(\bar{u}_{i,j} + \bar{u}_{j,i})$). $C_2$, $\sigma_k$ and $\sigma_\epsilon$ are modeling constants, while $C_1 = \max\left[0.43, \frac{\eta}{\eta+5}\right]$, for $\eta = \sqrt{2S_{ij}S_{ij}}\frac{k}{\epsilon}$ [10, 12, 13].

In combination with this turbulence model, a non-equilibrium wall function is used. This function performs well in flows with large pressure gradients, separating and re-attaching complex flows. Underneath the car, such complex flows can be expected [13].

### 2.2.2 Drag and lift coefficients

To determine the aerodynamic performance, a common method is to analyse the drag and lift coefficients. These are dimensionless coefficients defined by:

$$C_L = \frac{F_L}{\frac{1}{2}\rho v^2 A_L} \tag{2.9}$$

$$C_D = \frac{F_D}{\frac{1}{2}\rho v^2 A_D} \tag{2.10}$$

where $F_L$ and $F_D$ are the lift and drag forces, $\rho$ is the density of the fluid and $v$ is the velocity. $A_L$ and $A_D$ are reference areas. The drag and lift forces are calculated during simulation by integrating the pressure and the wall shear stress over the surface area of the body [13].

## 2.3 Governing equations solid

Similar to fluid systems, solid mechanics physics is governed by conservation of momentum, mass and energy. In order to solve this system of field equations, constitutive models have to be introduced. For the momentum equation, this could be a relation between stress and strain. One of the simplest models is Hooke's law, a linear model that for the general case reads:

$$\sigma_{ij} = C_{ijkl}\epsilon_{kl} \tag{2.11}$$

The momentum equation 2.3 is valid also for a solid element. For static equilibrium the momentum equation can be written as:

$$-\frac{\partial \sigma_{ji}}{\partial x_j} = \rho f_i \tag{2.12}$$

Multiplying with a test function and integrating over the volume of the element, a *weak formulation* of the problem can be derived. With a weak formulation of the equilibrium equation, the problem can then be solved using the finite element method.

For a nonlinear solver the internal forces (equivalent to membrane stresses) are taken into consideration in solving the displacements, to be able to give a more accurate deformation. The nonlinear problem is typically solved with an iterative method, for example with the Newton-Raphson method. For a more detailed theory and derivation of the equations, see for example [11, 14, 15].

## 2.4 The fluid structure interface

In fluids structure interaction, an important region is the interface surface which separates the fluid and the solid domain. At this surface, data is transferred between the coupled systems. In order to connect the governing equations from both the fluid and the solid, a set of coupling conditions are used at the interface surface. These conditions determine what kind of data is to be transferred. Given a non-conformal mesh, the data transfer require a mapping algorithm when passing quantities from one mesh type to another.

### 2.4.1 Coupling conditions

The boundary conditions at the interface surface, necessary for FSI problems, are governed by the so called kinematic and traction coupling condition.

In the kinematic coupling condition the fluid and the structure must have the same velocity/motion at the interface surface (recall the no-slip condition). At the same time, the traction condition makes sure the fluid and solid are in local equilibrium [5, 9, 16].

The kinematic condition can be fulfilled by choosing the fluid flow velocity equal to the time derivative of the solid displacement at the fluid structure interface wall [2]:

$$u_i = \frac{da_i}{dt} = \dot{a}_i. \tag{2.13}$$

$u_i$ here denote the fluid velocity, while $a_i$ are the displacement components at the solid boundary. For a steady state case, it is only necessary to make sure the displacements are equal:

$$d^f = d^s \tag{2.14}$$

where $d^f$ and $d^s$ are the displacement of the fluid and solid domain respectively, at the fluid structure interface surface.

The traction condition can be expressed by the stress (or force) balance between the fluid and the structure. Stresses can be represented by the so called *traction vector*, describing the force per unit area with normal $n_i$. The traction vector for the fluid and structure are seen in equation 2.15 and 2.16 respectively. In stress balance, these vectors will sum up to zero, as shown in equation 2.17 [2, 11].

$$t_i^f = -pn_i^f + \tau_{ij}n_j^f \tag{2.15}$$

$$t_i^s = \sigma_{ij}n_j^s \tag{2.16}$$

$$t_i^s + t_i^f = 0 \tag{2.17}$$

In a *partitioned* approach, the framework is usually meshed independently which creates a non-conformal mesh interface. The nodal positions of the fluid and solid mesh do not match the neighboring mesh. By using different mapping methods, such as interpolation and projection, it is possible to transfer the kinematic and the traction conditions between the fluid and structure frameworks [17].

Depending on if the transferred quantity is conservative or non-conservative, different methods of interpolation generally need to be applied. In the data transfer of System Coupling in Workbench for example, if a conservative quantity like mass and momentum is transferred, a method called *General Grid Interface* is applied. This method calculates weights that make the transferred quantity conserved locally. If all nodes are mapped correctly, the method is also globally conservative.

On the other hand, transferring a quantity like deformation, another method called *Bucket Surface Mapping* is used where the result does not need to be globally conservative. Rather, when mapping deformations, the *shape* of the surface should be preserved [18].

# 3

# Methodology

In order to reach the aim, a coupling of the fluid and structural solver was first created in a one-way setup. Thereafter the code was extended to include a two-way coupling. From start, Fluent was chosen as the fluid solver and MSC Nastran for the structural deformation. The softwares were chosen based on what was available at CEVT. To couple this system, pressure and displacement were the transferred quantities. The results were then compared to Ansys Workbench results.

## 3.1 FSI system overview

Coupling Fluent and Nastran in a partitioned FSI approach, was done using shell scripts and python subroutines. The overview of the coupling procedure can be seen in figure 3.1.

A main script in shell called each program in sequential order, starting with initialisation of the mesh. The commercial software ANSA was used to map the pressure onto the underbody panels. After calculating the deformations and stresses, $\mu$ETA post-processor was used to extract a *deformed* surface. This deformed mesh was used in the displacement transfer method in ANSA, where the CFD mesh was moved (*morphed*) in order to adjust for the deformation.

A convergence criteria was calculated at the end of the sequence to see if the pressure field and the deformation had stabilised between each iteration. This sequence then started over and iterated until convergence or maximum iterations were reached.

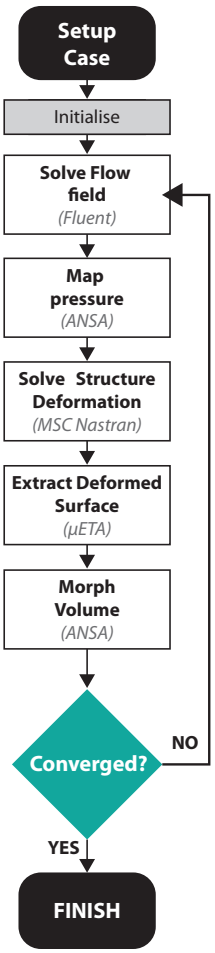


**Figure 3.1:** Script overview for two-way FSI.

## 3.2 Case setup

Two model geometries were created, one for the domain of the car and one for the structure of the panels. The model of the car was used to represent a real air flow around the panels while the structure of the panels was used for creating a realistic deformation.

### 3.2.1 Geometry

The car model was built up with a full car geometry, including body, wheels, underbody panels, fuel system and rear suspension. An older Volvo V40 was used as a reference for the design of the car body. The inside of the car was sealed off from the surrounding air.

In figure 3.2 the car geometry is presented.

(a) Car geometry.

(b) Front view.

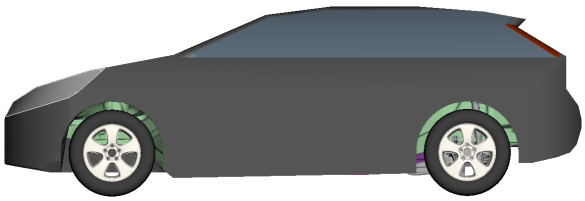

(c) Side view.

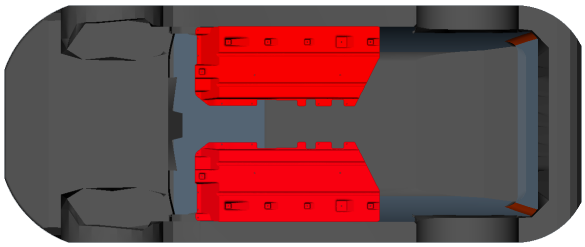

(d) Bottom view, showing the underbody panels and the car body.

**Figure 3.2:** Full car geometry.

In figure 3.3 it is possible to see two boxes that were created around the underbody panels. These boxes are used to separate the local volume around the panels, from the exterior fluid domain. This method simplifies the problem, so that two-way coupling only had to be considered locally around the panels.

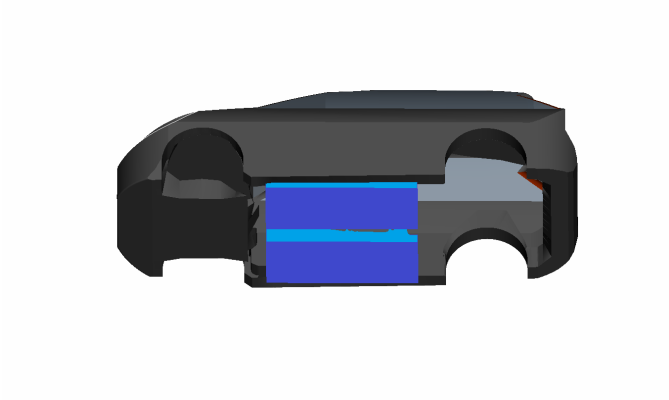

**Figure 3.3:** "Box-volumes" surrounding the underbody panels.

### 3.2.2 Mesh for fluid analysis

The CFD mesh around the underbody panels was created in ANSA using tetrahedral cells. The box-shaped geometry created around the panels seen in figure 3.3, formed the boundary of this tetrahedral mesh. The rest of the domain was meshed in Harpoon using a mainly hexahedral mesh. This method with two separated mesh types, made it possible to later only morph the tetrahedral mesh close to the panels.

The advantage of using ANSA for the tetrahedral mesh around the panels, was to obtain a high quality mesh around the panels for the morphing function. Tetrahedral cells were also supported by System Coupling in Workbench in order to transfer data. So called cut-cells with hanging nodes are not supported.

In order to mesh the box volumes around the panels, triangular meshes forming the boundaries of the boxes needed to be established. Since the geometry under the car was very complex, a method in ANSA called *inner wrap* was used. Like an inflating balloon, moulding to the surfaces, the general details of every component around each underbody panel were captured, forming a continuous surface mesh. The smallest element size of this mesh was set to 4 mm.

From the bottom side of each underbody panel, a prism cell inflation layer was created in order to capture boundary layer flow. The final mesh had five layers with a growth ratio of 1.2, where the first cell layer was 0.5 mm thick. The first cell layer was calculated to have a $y^+$ in the range between 30 to 100. It was approximated that the near-wall effects on the top of the panels had negligible impact. Therefore, there were no prism layers created above the underbody panels. The inflation layers can be seen in figure 3.4.

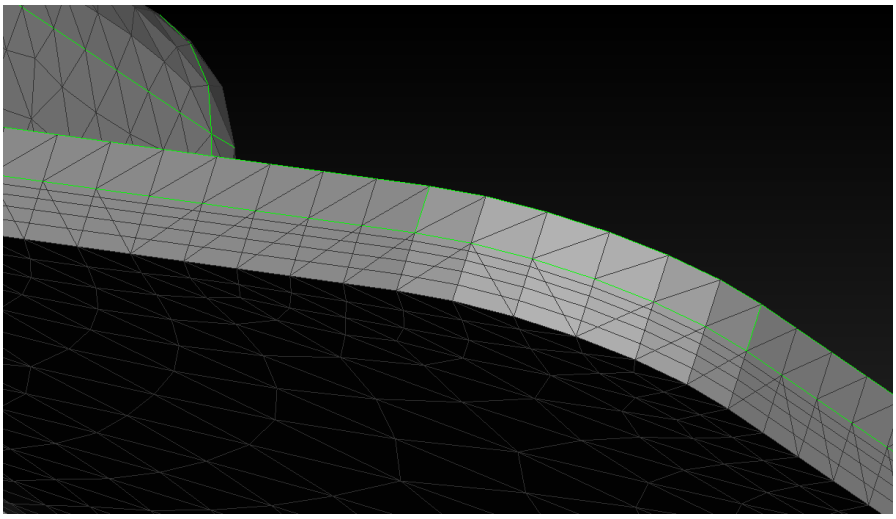

**Figure 3.4:** The prism cell inflation layers grown from the bottom of the underbody panels. A triangle/quad interface can be seen on the side of the five layers. This connects the boundary layer prism cells with the surrounding tetrahedral volume cells.

The hexahedral mesh created in Harpoon had smaller cell size below the car and around important details. Behind the vehicle where very turbulent flow was expected, a region of mesh refinement was added. For detailed settings used in Harpoon, see appendix A.1. All meshes were combined into one large mesh that can be seen in figure 3.5.

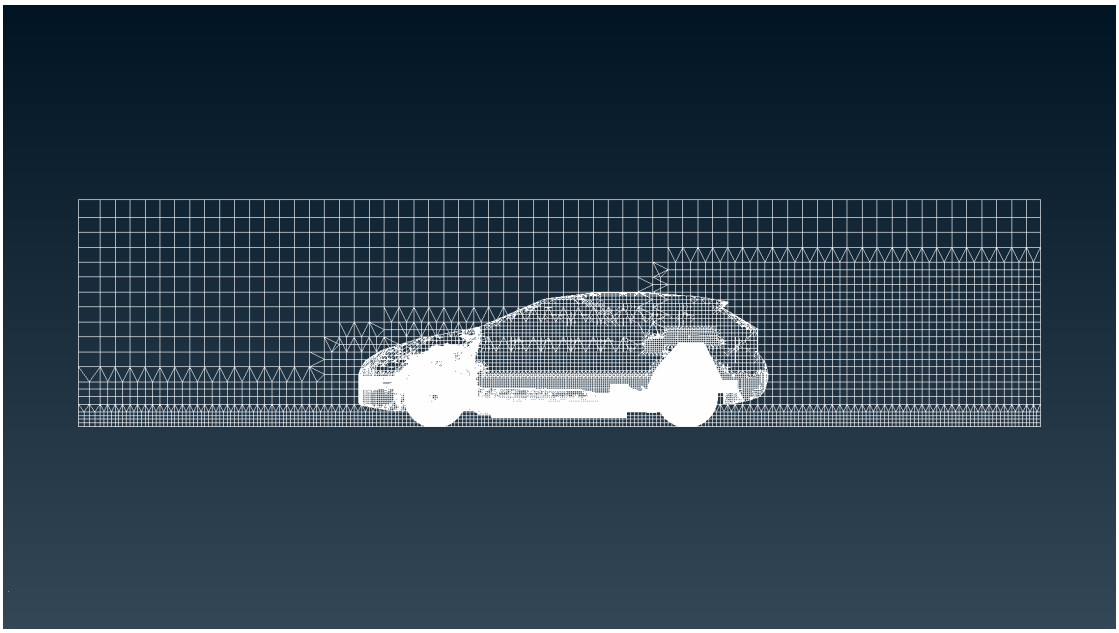

(a)

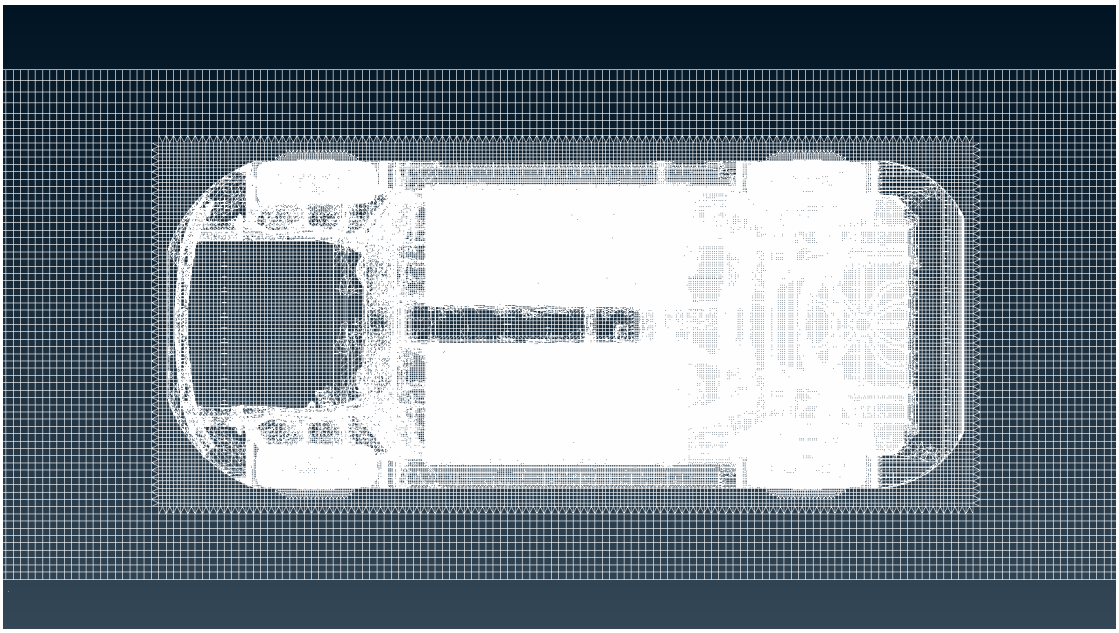

(b)

**Figure 3.5:** The final mesh combined from Ansa and Harpoon viewed from the side (a) and top (b). Total number of cells used was around 11 million.

### 3.2.3 Mesh for structural analysis

The underbody panels were represented by a mid-plane surface. On this surface a mainly quadrilateral shell element mesh was created with an average of 70 000 elements on each panel. The edge length of the elements were on average 4 mm, with finer mesh on curvatures to better preserve the geometry of the panels. A fine mesh also maintains the curvature of the surface when deforming the mesh. A coarser mesh with one fourth the total number of cells, was also produced to evaluate whether the results were mesh independent.

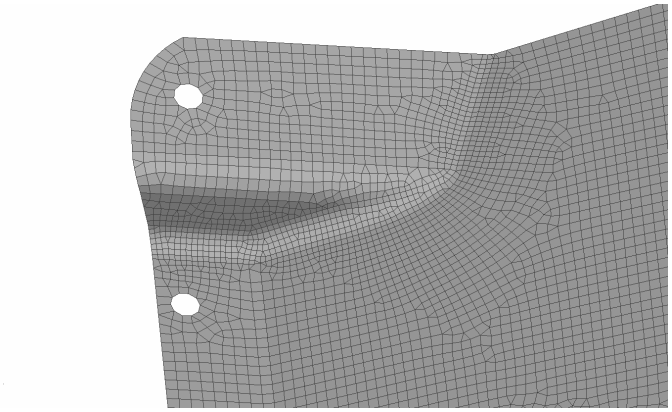

**Figure 3.6:** Hexahedral mesh of underbody panels.

## 3.3 Initialisation

The main reason for initialisation was to make sure all *property ID's* and *mesh nodes* had unique numbering, including both the CFD and FE mesh. This was important since both the FE mesh and the CFD mesh were imported together in ANSA when morphing. Nodes with the same ID would otherwise create conflicts.

## 3.4 Flow simulation

Fluent used a so-called *journal file*, containing commands for importing the mesh, setting relevant calculation models and to set boundary conditions. Fluent was initialised using a hybrid initialisation to make sure all cells had been assigned a value. This initialisation method was also used for assigning values to new or deformed cells. Afterwards an interpolation file was imported from an already converged solution. From this interpolation file the velocity, turbulence and dissipation were interpolated into the new mesh in order to reduce the number of iterations needed for convergence. To maintain a more stable solution between each coupling iteration, the solution started with first order accuracy on turbulence and dissipation. After 150 iterations, it was changed to second order accuracy.

Drag and lift coefficients were monitored on both the top and bottom surface of each panel. The history was stored in separate files for each coupling iteration. Contour plots were also used to plot the velocity and pressure underneath the car and on the panels. To export the pressure on the panels from the converged steady state solution, the surfaces had to be split into two separate walls using the *slit-wall-zones* function in Fluent.

For a complete list of important settings in fluent, see table B.1 in appendix.

## 3.5 Mapping

The mapping of the pressure onto the panels was done in the commercial software ANSA, using the *results mapping* function. This function took the static pressure and mapped it onto the quadrilateral mesh of the underbody panels, using a weighted average function. The weights are based on the area of intersection between the triangular (CFD mesh) and the hexahedral (FE mesh) mesh types. The program used the orientation of the pressure load, already defined in the CFD mesh, in order to map it correctly onto the FE panel. The mapping of the pressure can be seen in figure 3.7, where the load was applied in the direction of the arrows. The pressure was mapped on an *undeformed* structural mesh of the underbody panels.

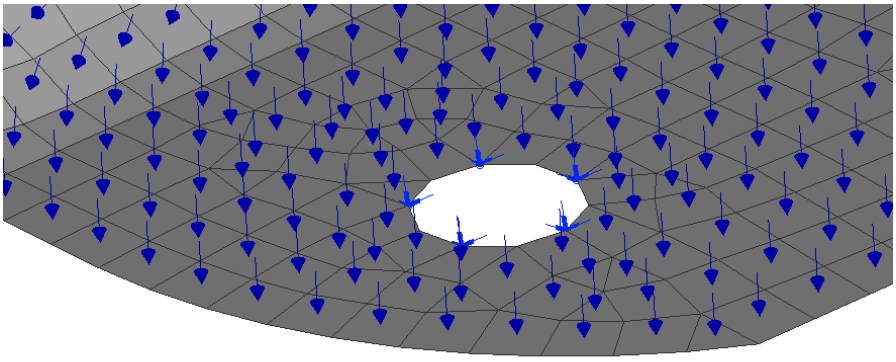

**Figure 3.7:** Mapping of pressure onto hexahedral mesh.

To linearly increase the pressure load mapped onto the structure, a ramping function was created using scripting in Python. This script read the mapped pressure data and rescaled it to make it increase linearly with the iteration number. This was used for the first coupling iterations in order to maintain a more stable deformation.

## 3.6 Structural simulation

The structural deformation of the underbody panels was computed in MSC Nastran. Nastran uses bulk data defined in the mapping step, such as pressure loads, defined grid points (nodes), shell elements and constraints. All mesh nodes located around the holes in the panels, were constrained in all six degrees of freedom as a fixed boundary condition.

The analysis solution sequence "SOL 106" was chosen. This is the static nonlinear solver in Nastran that can account for a re-distribution of pressure loads during deformation. The deformation calculated in Nastran was then exported in $\mu$ETA as a deformed mesh surface, used in the morphing function.

## 3.7 Morphing

With the deformations calculated, the CFD volume mesh was updated to match these deformations. Using a function called *surface fit* in ANSA, the mesh was morphed (as opposed to re-meshed) around the panels. As the name suggests, this method fits the undeformed panels in the CFD mesh onto the deformed surface FE mesh from Nastran and $\mu$ETA post-processing output. As the surface elements deformed, the volume elements followed.

A few nodes around the perimeter of the target and source surface were used in order to direct the morphing. Usually the minimum of three nodes was enough since the geometry was relatively simple. Only the local volumes around the panels (the box-volumes), were morphed. The walls of the box-volumes formed fixed boundaries of the movement.

During the morphing process, the mesh quality deteriorated. Mostly around corners and fine details in the geometry. The main reason was probably because of different element sizes in the two different meshes, or due to deformations being too large. In order to account for this, the automatic *fix quality* function of ANSA was used. Using predefined criteria for cell skewness and warping, ANSA performed local adjustment of node positions and reconstruction of critical cells to improve quality.

## 3.8 Convergence

In order to determine if the solution had converged, the changes in root mean square (RMS) values between each iteration were studied, eq. 3.1.

$$X_{RMS} = \sqrt{\frac{1}{N}\left(\sum_{i=1}^{N} X_i^2\right)} \tag{3.1}$$

where $X$ is the analysed values. In this project the convergence was calculated based on the pressure and the mesh node location. The total number of analysed values are defined by $N$. This RMS value was calculated for the pressure field exported from Fluent and on the mesh node locations from morphing. These values were then normalised with the RMS value calculated in the first iteration, eq. 3.2.

$$X_{i,Norm} = \frac{X_{i,RMS}}{X_{1,RMS}} \tag{3.2}$$

For each iteration, the difference in RMS value was calculated from the previous iteration. If the difference was lower than a user defined tolerance (see equation 3.3), the solution had converged and the iterations stoped. Otherwise the sequence started over, calculating a new pressure field in fluent.

$$\epsilon_{tolerance} < |X_{i,Norm} - X_{i-1,Norm}| \tag{3.3}$$

where $\epsilon_{tolerance}$ is the user defined tolerance.

## 3.9 Comparison in Ansys Workbench

In order to validate the results obtained from this fluid structure interaction coupling, the same case was setup in the commercial software Ansys Workbench. In Ansys Workbench the flow field was solved by Fluent and the structural deformation in Ansys Mechanical. These two solvers were then connected via a System Coupling component, which controlled the data transfer and the number of couplings steps used. Since it handled data transfer it also controlled whether the simulations were coupled one-way or two-way.

Figure 3.8 shows the components used for a fluid structure interaction setup in Ansys Workbench. This figure contains a static structural component (Mechanical) and a steady state fluid component (Fluent) which were both connected to the system coupling component. A converged solution was used for initialising the flow in Fluent. The structural mesh of the underbody panel was imported through the external model component.

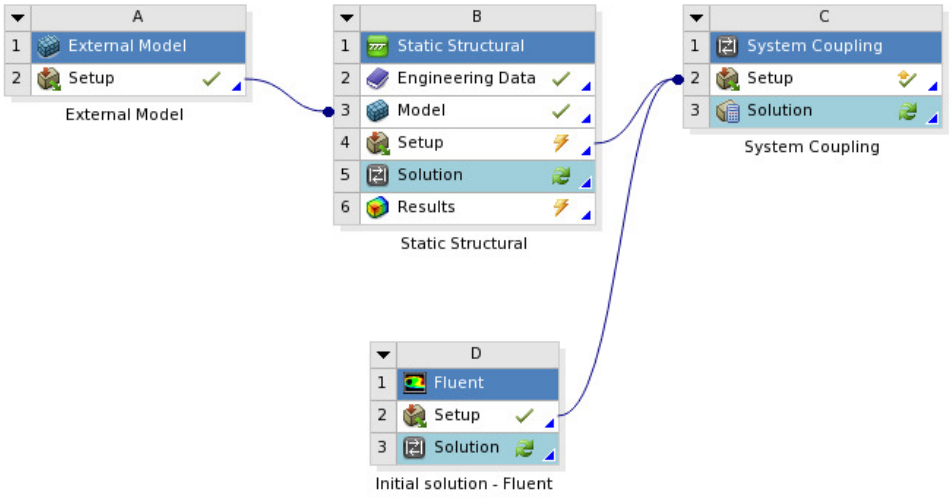


**Figure 3.8:** Setup in Ansys Workbench. Specific settings in the system coupling component controls whether one-way or two-way coupling is performed.

To be able to import the pressure onto both sides of the underbody structural mesh, the panels were split into two identical mid-surfaces. These two surfaces had a thickness that grew in opposite directions, with half the original thickness each, see figure 3.9. These two mid-surfaces were glued together through a *bonded* contact condition.

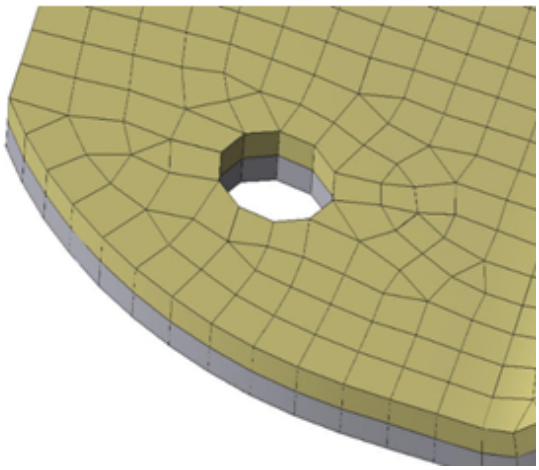

**Figure 3.9:** Split mid-plane surface used in Ansys Workbench.

To allow the mesh to move in a two-way simulation, the *dynamic mesh* function in Fluent was activated. For this problem, a diffusion based movement was used.

# 4

# Results

## 4.1 General flow field

The general flow field around the car can be seen in the velocity contour figure 4.1. The flow field shows accelerated flow above and below the car, due to conservation of mass. The figure also confirms that the rotational speed of the wheels is set correctly. There is no airflow inside the enclosed car and the flow is almost stationary in the engine bay. The simple engine shield directs the flow past this cavity. At the rear of the car, a flow separation occurs, creating a wake with circulating turbulent air.

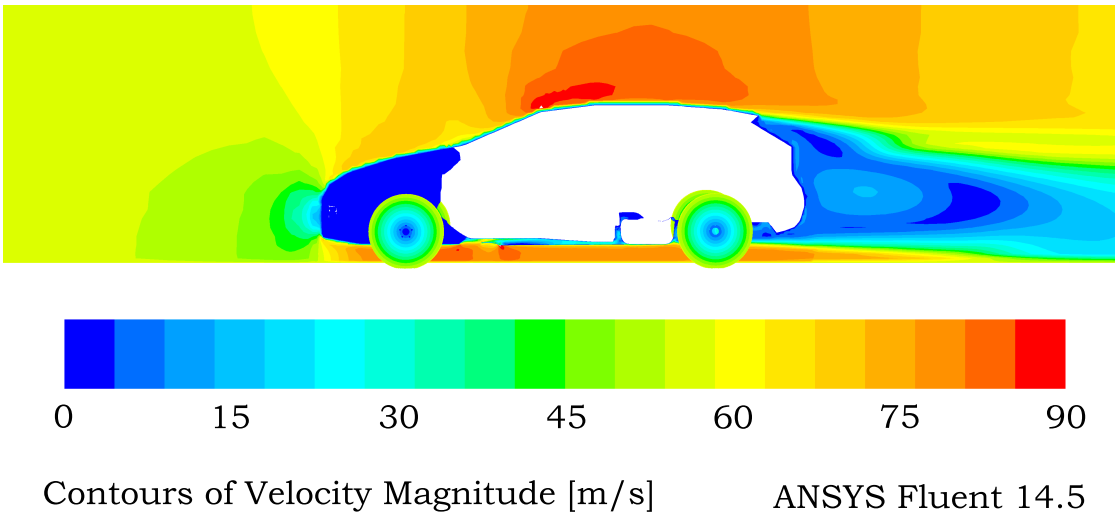


**Figure 4.1:** A plane cut through the car showing the flow field around the car.

The flow reaches a velocity of around 75 m/s under the car, compared with the inlet velocity of 55 m/s. Above the panels, the flow has a velocity between 0 - 25 m/s. The panels were moved downwards in order to make the model fit the car geometry. This created a leakage at the leading edge of the panel which can be seen in figure 4.2.

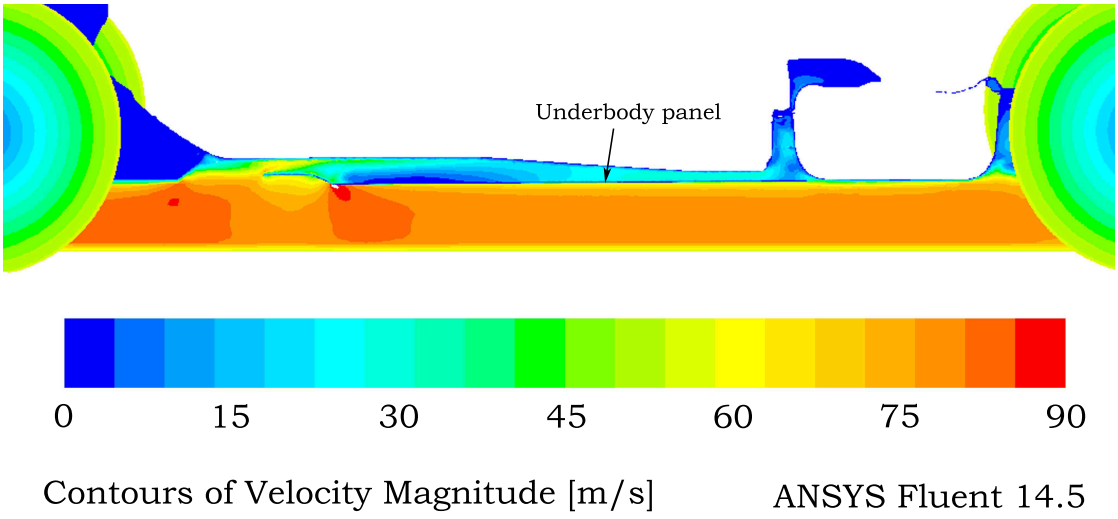


**Figure 4.2:** Flow field around the underbody panels.

The static pressure distribution around the car can be seen in figure 4.3. The top side of the panel shows a mean static pressure distribution of around $-1000$ Pa (relative to 1 atm operating pressure), which can be seen in figure 4.3(a). This under-pressure on the top side creates a force that wants to deform the panels upwards. The overall pressure on the bottom side of the panel is similar to the top side, giving a force that deforms the panel downwards, see figure 4.3(b). For the bottom side of the panel, an overpressure can be seen in the bottom left corner at the front of the panel, where the flow is deflected around a geometric feature in the panel.

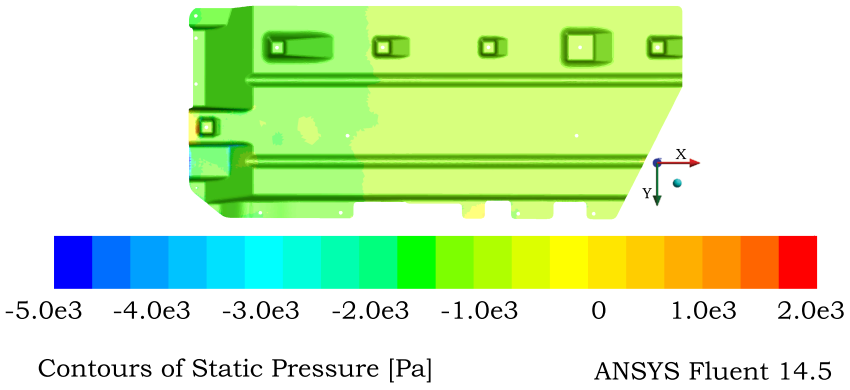


(a)

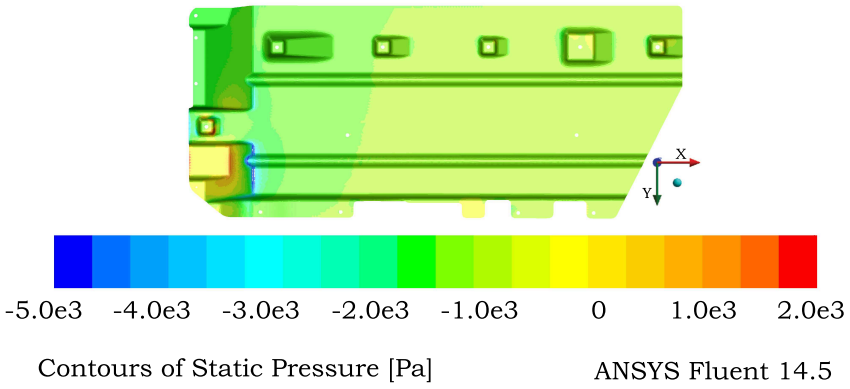


(b)

**Figure 4.3:** Static pressure distribution on the left underbody panel viewed from below. Pressure on the top side (a), and pressure on the bottom side (b) is the gauge pressure relative to the operating condition (at 1 atm).

The flow right below the underbody panels, is shown in figure 4.4. The black rectangles mark the locations of the underbody panels. The wheels slow down the air and creates wakes of high turbulence that affect the panels locally.

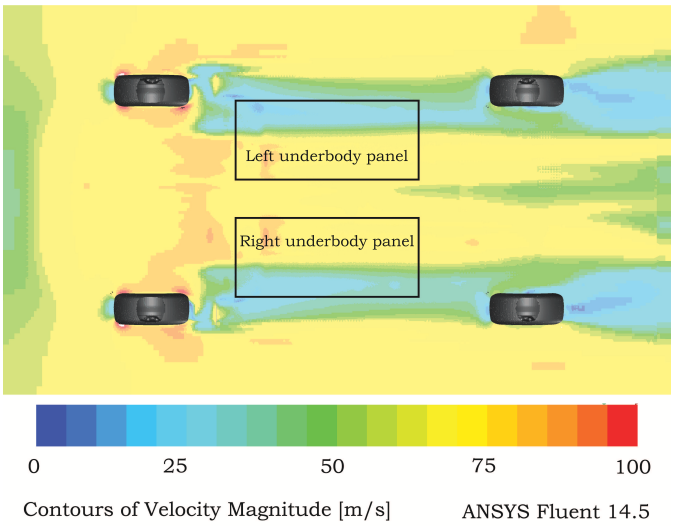


**Figure 4.4:** Flow field underneath the car. The black rectangles mark the locations of the underbody panels.

## 4.2 One-way simulations

In the one-way coupling, the static pressure from the general flow field was mapped onto the underbody panel FE mesh. The resulting deformations and stresses are shown and compared below. In order to verify the results of the Fluent-Nastran FSI coupling, Ansys Workbench was used to make sure the results were reasonable.

### 4.2.1 Deformation

Figure 4.5 shows the deformation of a coarse mesh (a) and a fine mesh (b), both calculated using Mechanical in Workbench. Using a finer mesh results in a slight increase in maximum deformation, going from 0.26 mm to 0.28 mm. Maximum deformation occurs at the leading edge in both models.

Figure 4.5(c) shows the deformation of the panel for a one-way coupling in the FSI script using Fluent and Nastran, with a maximum deformation calculated to 0.25 mm. The mesh was the same fine mesh as was used in 4.5(b). An almost identical displacement profile can be seen between the deformation in Mechanical and Nastran, with a maximum deformation difference of 0.03 mm.

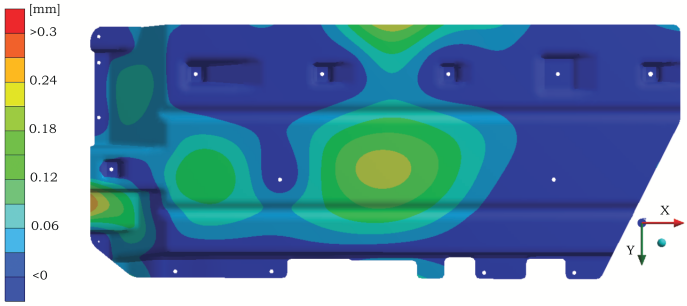


(a)

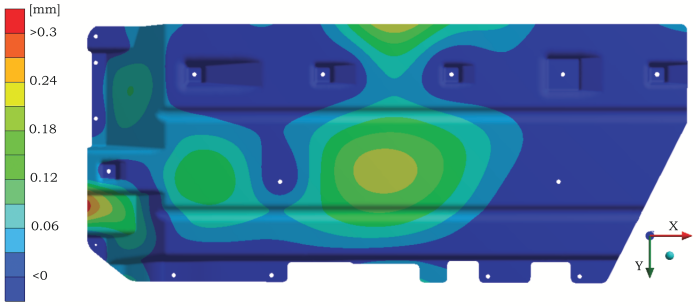


(b)

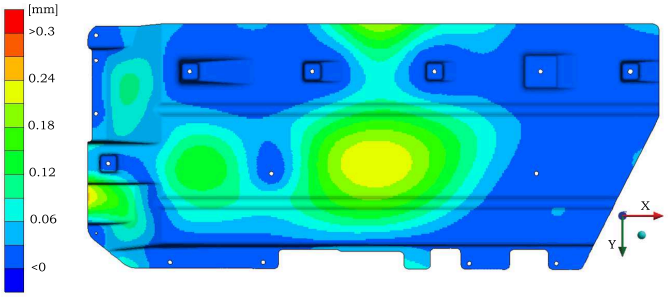


(c)

**Figure 4.5:** Total deformation from one-way simulations. Coarse mesh results from Mechanical (a), fine mesh results from Mechanical (b) and fine mesh results from Nastran (c).

### 4.2.2 Stress distribution

Figure 4.6(a) and 4.6(b) show the distribution of von Mises stress on the coarse and the fine mesh respectively from simulation in Mechanical. The maximum stress for the coarse mesh is 1.9 MPa and for the fine mesh it is 3.0 MPa. It is of importance to note that the maximum von Mises stress is far from the yield limit which is estimated from material tables to *at least* 30 MPa.

Figure 4.6(c) shows the corresponding von Mises stress distribution from the MSC

Nastran simulation. The maximum von-Mises stress is calculated to 3.2 MPa compared to 3.0 MPa from Ansys Mechanical.


(a)

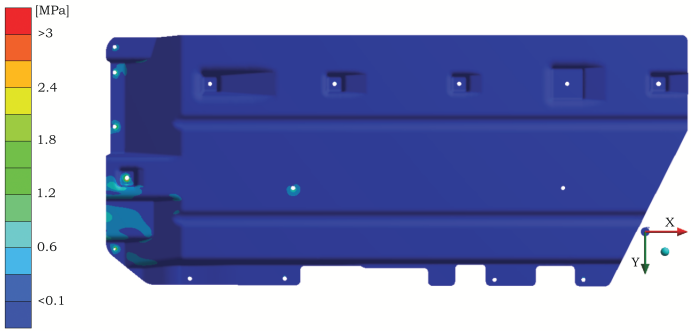


(b)

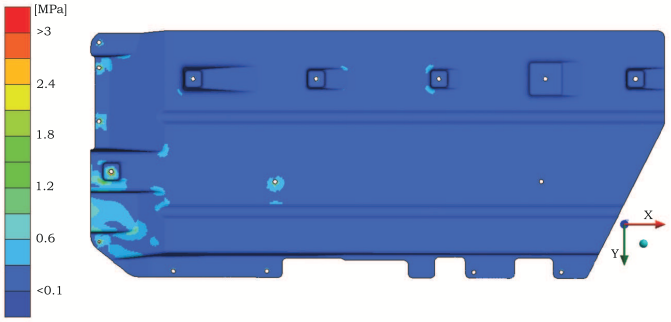


(c)

**Figure 4.6:** Stress distributions from one-way simulations of the left panel viewed from below. Coarse mesh results from Mechanical (a), fine mesh results from Mechanical (b) and fine mesh results from Nastran (c).

The maximum stress distribution occurs at the leading edge of the panel for both the results from Mechanical and Nastran. A close-up view showing the stresses at the leading edge of the panel is shown in figure 4.7.

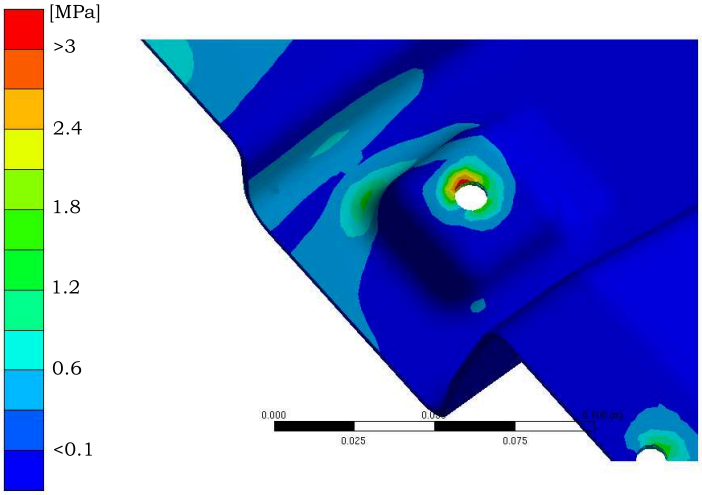


**Figure 4.7:** Close-up view of the left underbody panel leading edge, showing the stress distribution of the fine mesh (one-way simulation) from Ansys Mechanical.

## 4.3 Two-way simulations

The simulation was then set up for two-way coupling and the results are presented below. The script executing the Fluent-Nastran coupling ran for 30 iterations.

### 4.3.1 Deformation

In figure 4.8 the displacement is shown for the first six coupling iterations. The pressure load is increased linearly up to the fifth iteration. From the fifth iteration and onward, full load is applied.

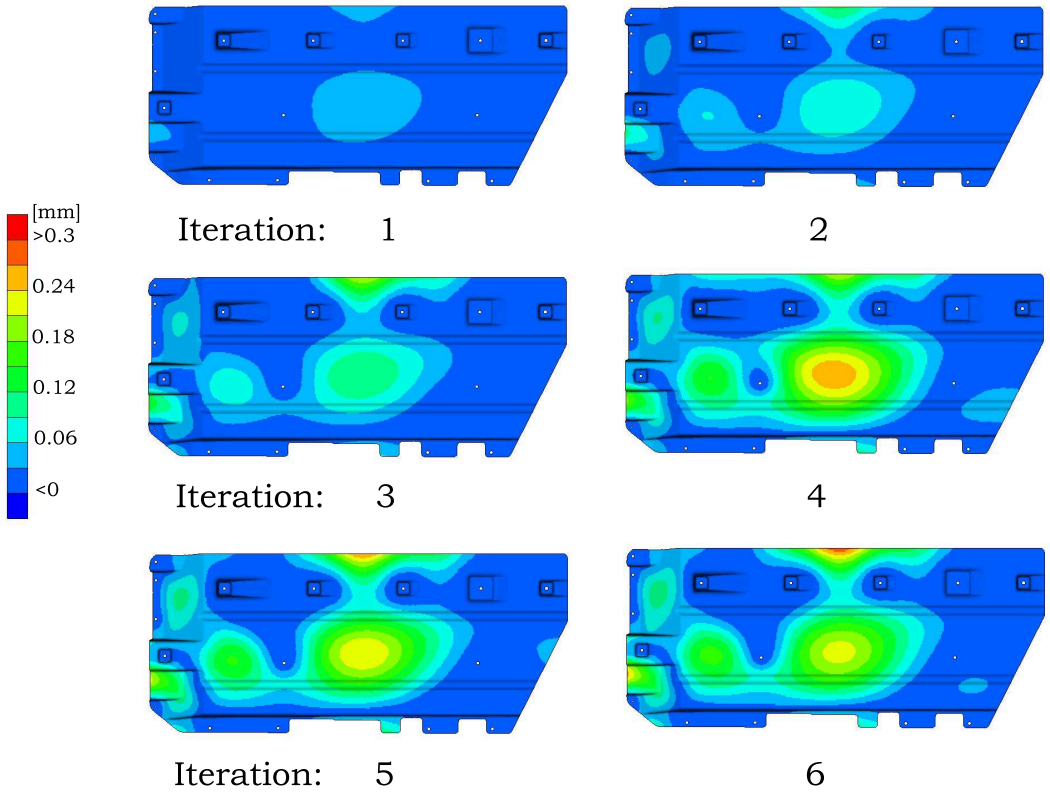


**Figure 4.8:** First six coupling iterations including a linear pressure ramping during iterations (1-5). Full pressure force is applied from iteration five.

The two-way coupling results are shown in figure 4.9 for Fluent-Nastran FSI. The deformation of the panel is displayed for iterations 14-21. This shows that the two-way coupling deformations oscillate back and forth, with an amplitude of around 0.05 mm. A converged result for the two-way coupling should therefore have a maximum deformation in the range of 0.2-0.3 mm.

Another interesting observation is that the two-way simulations have the maximum deformation located at the centre of the panels. One-way deformations on the other hand always have the maximum deformation located at the leading edge (figure 4.5).

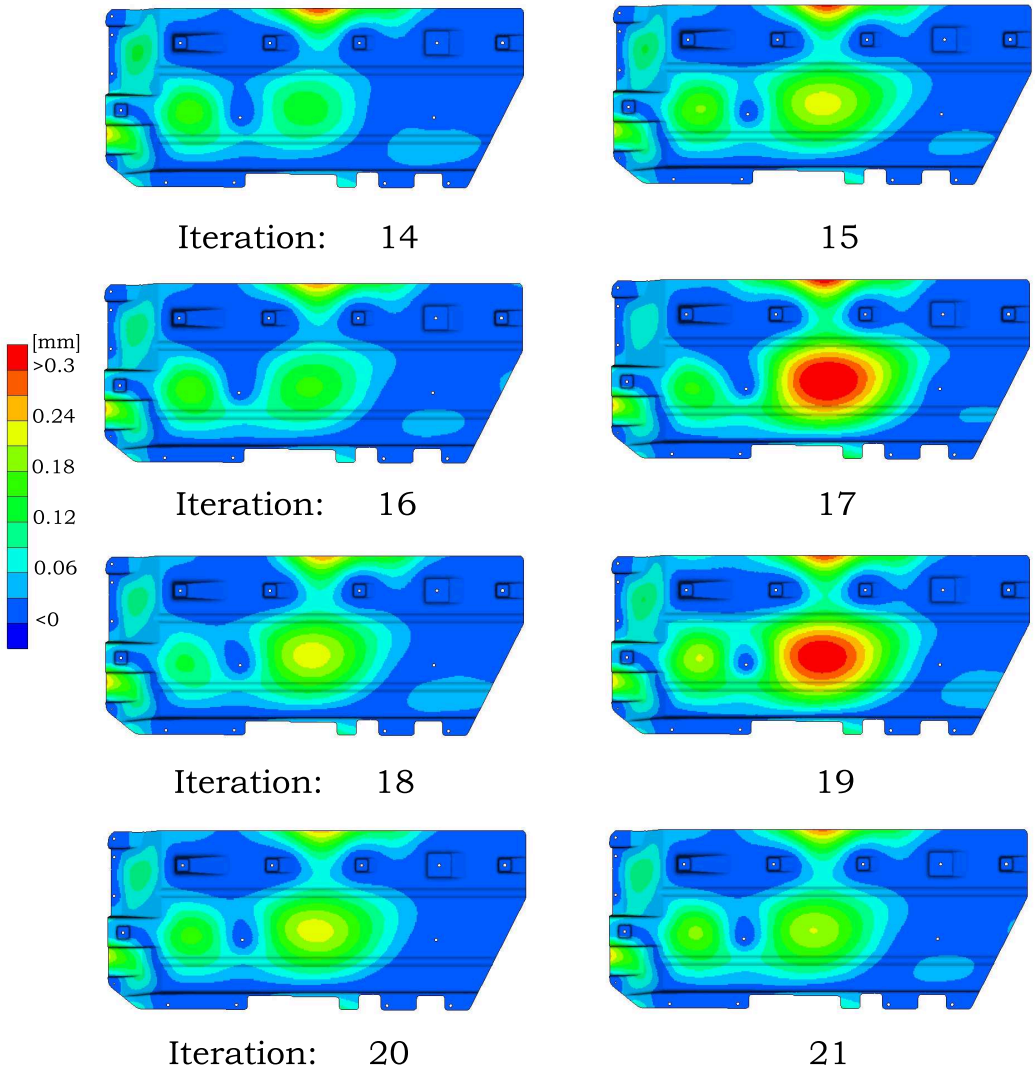


**Figure 4.9:** Two-way coupling iteration 14-21 for FSI using the Fluent-Nastran script.

Figure 4.10 shows iterations 22-27. Iteration number 23 has a very large displacement compared to the rest of the iterations. This is because the flow field did not converge. In iteration 22 a normal distributed displacement can be seen, before the rapid change in pressure and displacement occurs in iteration 23.

It is also seen that the large change in displacement has an impact on a few of the iterations that follow, for example on iteration 24 and 25, before the deformed profile becomes normal again.

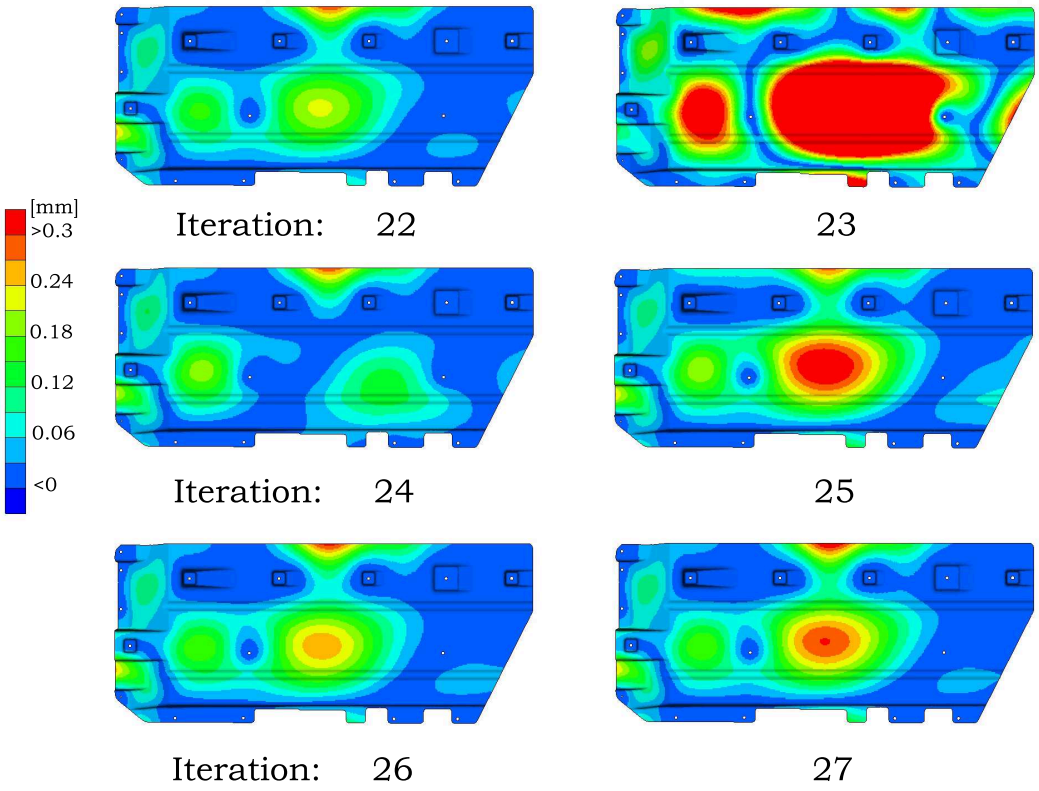


**Figure 4.10:** Panel displacement from iteration 22 - 27.

### 4.3.2 Stress distribution

The stress distribution from two-way simulations gave similar results as in one-way simulations. The maximum von-Mises stress is far from the yield limit and only has small fluctuations between every coupling iteration.

### 4.3.3 Changes in drag and lift

Each iteration the lift and drag coefficients were calculated. These results are compared with the coefficients for an undeformed panel in figure 4.11(a) and 4.11(b) respectively. The drag and lift coefficient were calculated based on standard atmospheric pressure (1 atm) with an reference area of 1 $m^2$ and an air flow velocity of 55 m/s.

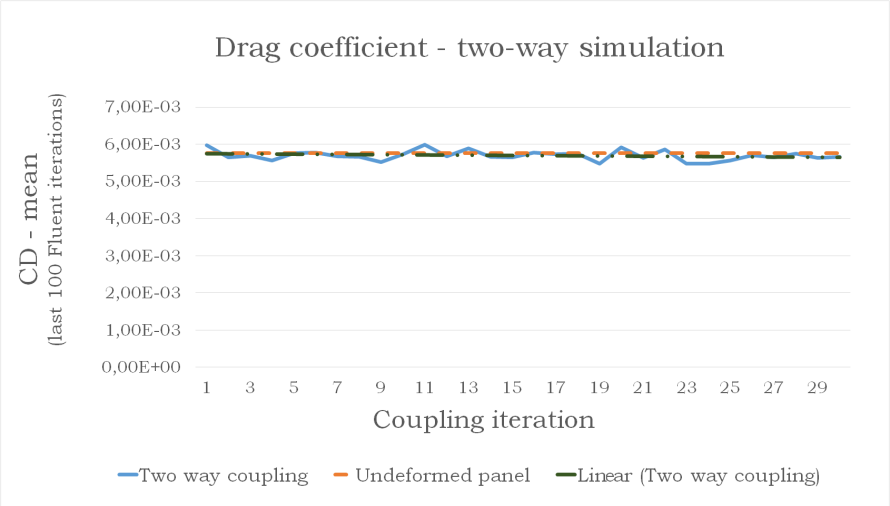


(a) Calculated drag coefficient in the two-way simulation (solid line). The drag coefficient for an undeformed panel (dashed line) is 0.0058. The dotted line shows a linear trend line of the two-way iteration values.

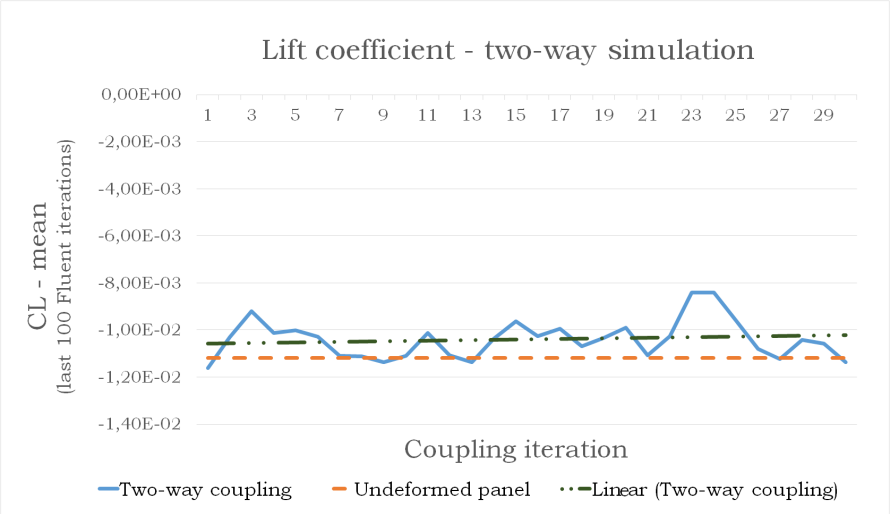


(b) Calculated lift coefficient (solid line) compared with the coefficient for an undeformed panel (dashed line). The undeformed panel lift coefficient has a value of 0.011. The dotted line is a linear trend line of the iterations for the two-way result.

**Figure 4.11:** Two-way simulation drag coefficient history (a) and lift coefficient history (b).

The drag coefficient of the undeformed underbody panel was found to be 0.0058. The results of the $c_d$ calculation from the two-way simulation show no major change from that value.

The lift coefficient $c_l$ of the undeformed panel was computed to 0.0112. The two-way simulations showed that the fluctuations in lift coefficient are slightly larger and that there could be a trend towards an increased value.

### 4.3.4 Convergence

The RMS convergence of the pressure field and the displacement are calculated for the Fluent-Nastran two-way simulation and shown in figure 4.12 and 4.13 respectively. The way the RMS values were calculated, they should go towards a limit as the iterations progress if the solution converges.

Figure 4.12(a) shows the pressure convergence on the top side of the left underbody panel. Because of fluctuations in the results, the pressure field has not converged. Note especially iteration number 23, where the RMS value rapidly decreases. This is because of the non-converged solution presented before in figure 4.10.

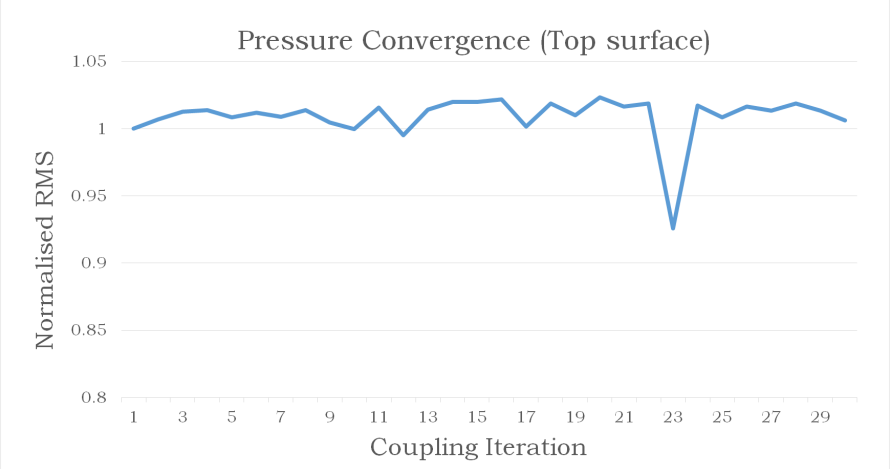


(a)

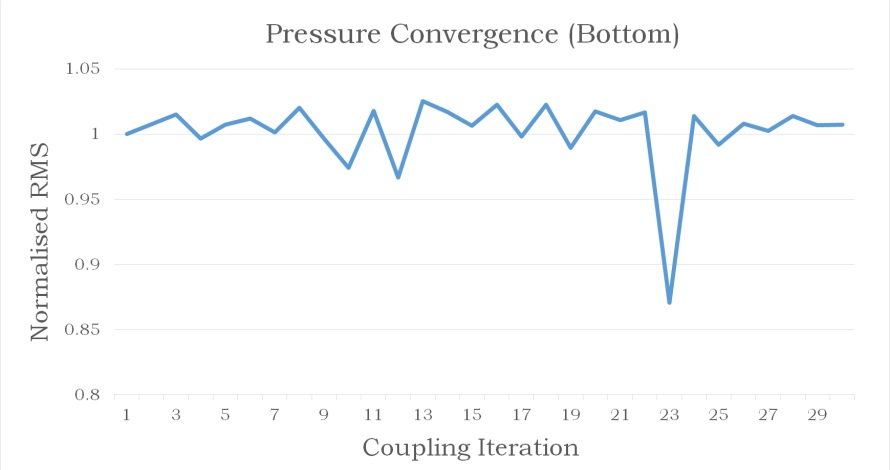


(b)

**Figure 4.12:** Pressure convergence at the top surface (a) and at the bottom surface (b) of the panel.

Figure 4.12(b) shows the pressure convergence at the bottom side of the panel. This result displays a similar pressure convergence as the top-side. The same rapid decrease in pressure on iteration 23 can also be seen for the bottom side of the panel.

Figure 4.13(a) shows the displacement convergence at the top side of the panel. Note the small scale of the axis, showing that the fluctuations in RMS value during the iteration process are very small.

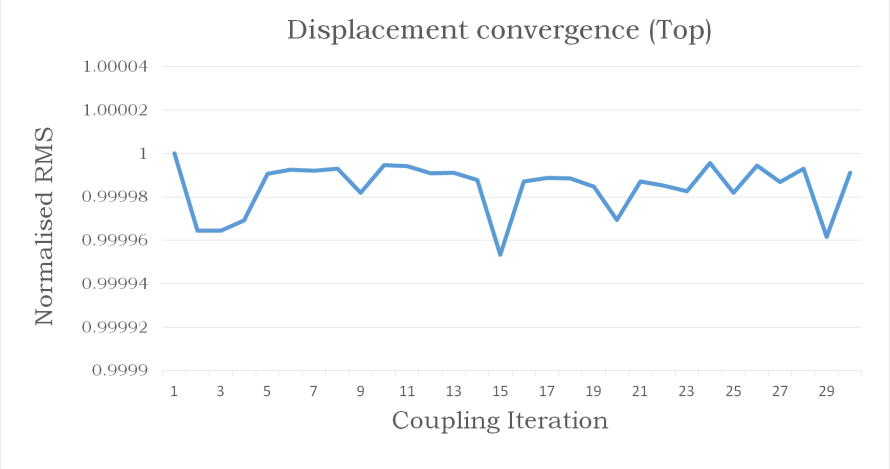


(a)

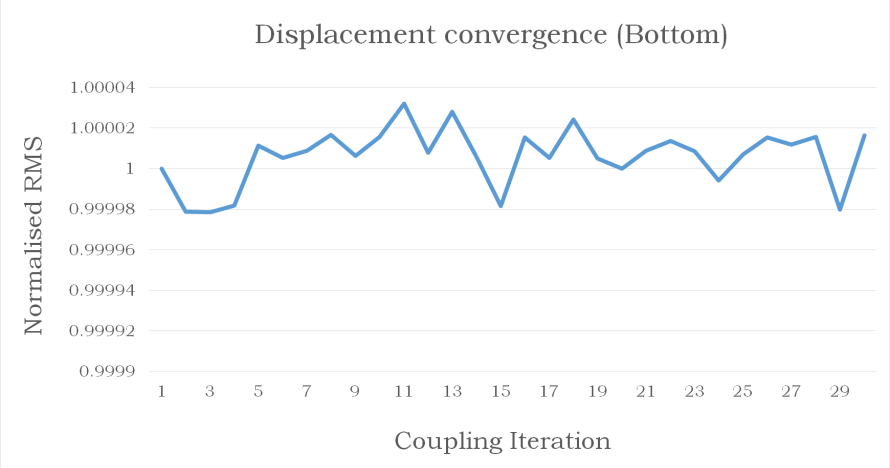


(b)

**Figure 4.13:** The displacement convergence at the top (a) and at the bottom (b) side of the panel.

Similarly, figure 4.13(b) shows the displacement convergence at the bottom side of the panel. It is interesting that the displacement convergence is not completely similar to that of 4.13(a), even though the bottom and the top side of the panel should have

exactly the same mesh node locations. The difference in mesh node locations, probably comes from the *slit-wall-zones* function in Fluent.

Note also that there is no significant change in RMS value of the displacement in iteration 23, as was previously shown for the pressure (figure 4.12).

## 4.4 Time distribution in the FSI system

Figure 4.14 shows the time distribution of the different steps in the two-way FSI coupling script, for one iteration. The time spent for an entire coupling iteration (not counting the initialisation) was around two hours. The initialisation step is only performed once during the start-up. The Fluent simulation takes around 90 minutes but this time can easily be reduced by increasing the number of computational cores. Nastran simulation time is mainly reduced by properly setting up the nonlinear parameters. Mapping is very fast while morphing is very time consuming since it imports the entire mesh but only morphs a small part of it.

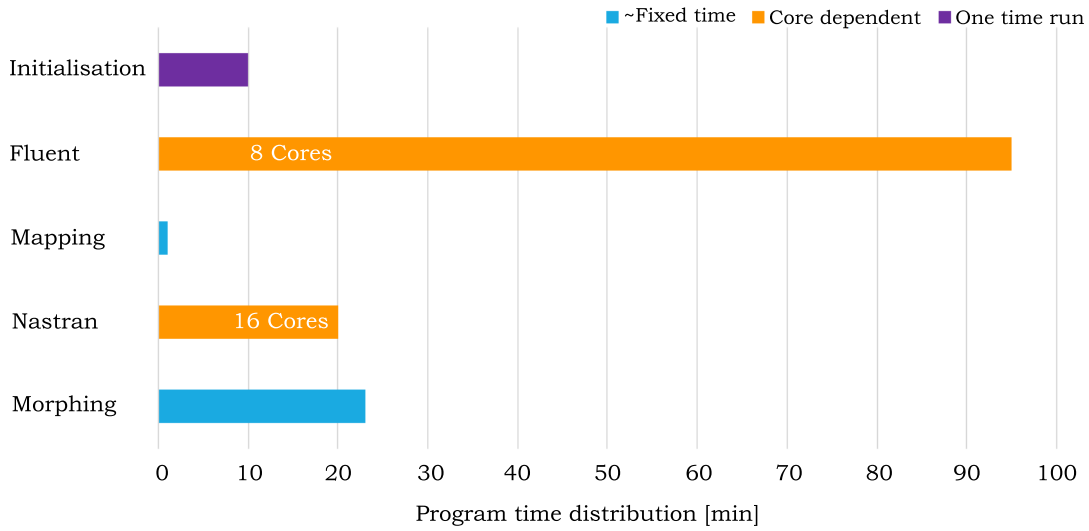


**Figure 4.14:** Time distribution for the script based Fluent-Nastran two-way coupling.

# 5

# Discussion

Our model resulted in a flow profile around the car, that as expected had higher velocity around the car compared to the inlet velocity. This because of mass conservation. However, due to misalignment of the geometry (still under development at CEVT), the underbody panels were lowered in order to fit in the model. This resulted in a leakage at the leading edge of the panels, creating an error in the pressure distribution.

The entire car model was used for simulation of the flow around each panel. This resulted in only small pressure differences between the two panels. To decrease the model size, it would have been a good enough approximation to only consider one panel and half the car geometry. Also, some issues with convergence were experienced. Especially behind the vehicle in the turbulent region, and in some bad quality cells. With a smaller domain, further refinement could have been done in these areas without affecting the total number of cells, and would have better resolved the turbulent flow.

For the one-way simulations, the comparison between the coarse and the fine mesh in Ansys Mechanical was first performed. It shows that a four time increase in total number of cells, resulted in only a 0.02 mm increase in maximum deformation. This indicates a mesh independent result. When comparing the simulation in Nastran with Mechanical, the difference was only 0.03 mm and the deformation profile was almost identical. From the similar results in Nastran and Mechanical, the conclusion is drawn that the FSI script was set up properly for handling two-way simulations.

The results from the two-way simulations with the FSI script, show that the deformation of the underbody panel oscillate during the static analysis. This is a clear indication of a convergence issue in the method. It also verifies that a partitioned approach is an unstable FSI procedure. If a stable solution to this problem exist, it should be within the range of the maximum and minimum deformation. Since the deformations are small, a one-way simulation would have been enough.

To reduce oscillations in the beginning of a simulation, due to applying the full pressure on an undeformed underbody panel, a ramping function was implemented.

However, to solve the convergence issues after the initial ramping, a damping function (using for example under-relaxation) would have been needed.

Stress distributions in both one-way and two-way simulations are very similar. The small deformations lead to small stresses and the results show no risk of plastic deformation.

There is no significant impact on drag and lift coefficient between an undeformed panel and the two-way simulation, because the deformations are too small. The fluctuations seen in figure 4.11 are most likely to be numerical instabilities due to convergence issues in the flow field.

The RMS values and convergence criteria were calculated based on the pressure and displacement (mesh node location). This process was implemented in order to have a fast and simple way to check whether the solution had converged. A number of indicators in the results showed that this method had some issues. For example, the displacement convergence (figure 4.13) indicates a converged solution while the deformation still changed every iteration (see figure 4.9).

This is also related to the issue where the largest displacement in the two-way coupling simulation, in iteration 23 from figure 4.10, did not show any change in RMS value of the displacement at all. The reason is that the RMS value is calculated based on all coordinates: x, y and z, while the very small deformation mainly took place in the z-direction. Therefore, a change in one coordinate is not likely to be seen in a RMS value over *all* coordinates.

Another example is that the top and bottom side of the panel do not have identical mesh node convergence, see figure 4.13. This error is probably due to the *slit-face-zone* function in Fluent, that separates the underbody panel mid-surface into two uncoupled wall zones, that does not share the same mesh node coordinates.

A better method for calculating the convergence criteria would be to base the RMS value on the *pressure difference* and the *change* in mesh node coordinates between each iteration. The node coordinates should be taken from the deformed surface extracted from $\mu$ETA, instead of the slit surface from Fluent. However this method was more complex to implement and not suitable within the time frame of the project.

One of the most difficult areas in the FSI script was the morphing. The morphing function used was not robust enough and could only handle small deformations. In order to get a good quality CFD mesh after morphing, the mesh had to be heavily improved after each morphing step. This was not ideal since the user lacks control of the automated mesh improvement function in ANSA. To handle larger deformations the morphing function has to be updated, taking into consideration a local volume re-mesh. All things considered, the current morphing function in ANSA is not recommended.

For this project, where the deformations were small, the pressure forces were mapped onto an *undeformed* structural mesh. In the two-way FSI coupling however, the pressure is calculated on the *deformed* underbody panel. Since these do not overlap, the pressure will not be fully mapped. The mapping process is thus not conservative and does not fulfill the traction boundary condition requirement in FSI, where the stresses are equal at the interface surface.

By the same principle, the displacements are not *mapped* from the structural mesh to the CFD mesh. Instead the *surface fit* method was used in morphing, where the profile of the underbody panels is not preserved. For example, how can a fine mesh fit on a coarse mesh, or the other way around? This violates the kinematic condition, since the positions of the panels are not entirely the same.

# 6

# Conclusion

In fluid structure interaction the mesh setup is of high importance, especially at the fluid structure interface. The mesh needs to be able to preserve the surface of the structure as well as map the displacement and the pressure correctly. A robust morphing function is also needed to connect the FSI method into a two-way coupling.

The results obtained from both one-way and two-way FSI simulations show that there is no significant change in drag or lift coefficient of the underbody panels, because the deformations are too small. The maximum deformation of the underbody panels are in the range of 0.2-0.3 mm. Combining this with the fact that the stresses are small, with a maximum stress of around 3.0 MPa, there is a possibility to use thinner panels in future cars. More thorough investigation have to be done with transient simulations to evaluate the dynamic behaviour of these thinner panels.

In order to have a fast and robust two-way FSI method, the most important areas of improvement lie within the setup of the case and the morphing function. These two processes are currently the most time demanding and unreliable. The morphing function used in this project is not recommended and an improved method could not only speed up the process but also be able to handle larger deformations. This can be done by using other commercial software or developing a new script. Improvements could also be done on convergence and mapping functions.

The one-way FSI script method is very easy to implement and a good method to analyse deformation and stresses. It gives an early indication to whether larger deformations are present and if two-way FSI is needed. For the underbody panels, were the deformations are small, a one-way coupling is sufficient. Underbody panels could still experience larger deformation if the surrounding medium is changed, for example air to water, which could lead to larger forces.

For future analysis of underbody panels and other systems with small deformations, transient simulations could still be relevant. Oscillations in systems, noise and failure due to vibrations are important to consider.

# Bibliography


[1] Y. Bazilevs, K. Takizawa, T. E. Tezduyar, Computational Fluid-Structure Interaction: Methods and Applications, Wiley, 2012.

[2] O. C. Zienkiewicz, R. L. Taylor, P. Nithiarasu, S. (e-book collection), The finite element method for fluid dynamics, Butterworth-Heinemann, Oxford, 2014.

[3] F.-K. Benra, H. J. Dohmen, J. Pei, S. Schuster, B. Wan, A comparison of one-way and two-way coupling methods for numerical analysis of fluid-structure interactions, Journal of Applied Mathematics 2011.

[4] Archives of Computational Methods in Engineering 20 (3).

[5] F. Axisa, J. Antunes, B. E. (e-book collection), Modelling of mechanical systems: Vol. 3, Fluid-structure interaction, Elsevier/Butterworth-Heinemann, Amsterdam; Boston, 2007.

[6] J. Degroote, K.-J. Bathe, J. Vierendeels, Performance of a new partitioned procedure versus a monolithic procedure in fluid–structure interaction, Computers and Structures 87 (11) (2009) 793–801.

[7] H. G. Matthies, J. Steindorf, Partitioned strong coupling algorithms for fluid–structure interaction, Computers and Structures 81 (8) (2003) 805–812.

[8] V. V. S. Vytla, Y. Ando, Fluid structure interaction simulation of fuel tank sloshing (04 2013).
URL `http://dx.doi.org/10.4271/2013-01-0641`

[9] C. Kleinstreuer, S. O. service), Modern Fluid Dynamics: Basic Theory and Selected Applications in Macro- and Micro-Fluidics, Vol. 87, Springer Netherlands, Dordrecht, 2010.

[10] L. Davidson, Fluid mechanics, turbulent flow and turbulence modeling, lecture notes in msc courses, Tech. rep., Chalmers University of Technology, Göteborg (2014).

[11] S. Toll, M. Ekh, Mechanics of solids & fluids. part i: Fundamentals., Tech. rep. (2013).

[12] T.-H. Shih, W. W. Liou, A. Shabbir, Z. Yang, J. Zhu, A new k-$\epsilon$ eddy viscosity model for high reynolds number turbulent flows, Computers and Fluids 24 (3) (1995) 227–238.

[13] Ansys Inc., Ansys Fluent Theory Guide.

[14] N. Saabye Ottosen, H. Petersson, Introduction to the finite element method, Prentice Hall, New York, 1992.

[15] F. Larsson, Non-linear finite element analysis, a short introduction, Tech. rep., Chalmers University of Technology, Göteborg (2010).

[16] H.-J. Bungartz, M. Schäfer, Fluid-Structure Interaction: Modelling, Simulation, Optimisation, Springer-Verlag, 2006.

[17] R. Jaiman, H. Thomas, F. Shakib, Direct-coupled fluid-structure interaction for automotive applications (04 2012).
URL `http://dx.doi.org/10.4271/2012-01-0760`

[18] Ansys Inc., System Coupling User's Guide.

# A

# Harpoon - settings

**Table A.1:** Settings for Harpoon mesher.

| | |
|---|---|
| base level ≡ level (1) | 40 mm |
| Part | Part level (cell size) |
| body | 2 (20 mm) |
| wheels | 4 (5 mm) |
| fuel system | 4 (5 mm) |
| rear suspension | 4 (5 mm) |
| road | 1 (40 mm) |
| wake refinement zone | 1 (40 mm) |
| road refinement zone | 2 (20 mm) |
| underbody panel refinement zone | 3 (10 mm) |
| mesh type | hex |
| expansion | slow |

# B

# Fluent - settings

**Table B.1:** Settings in Fluent solver.

| Solver settings | |
|---|---|
| solver | pressure-based, steady state |
| turbulence model | realisable $k$-$\epsilon$ |
| wall function | non-equilibrium |
| pressure-velocity coupling | coupled scheme |
| $k$, $\epsilon$ and momentum discretization | first order upwind (start) |
| | 2nd order upwind (after $\approx$ 150 iterations) |
| flow courant number | 20 |
| initialisation | hybrid and interpolated converged solution |

| Boundary conditions | |
|---|---|
| road speed | 55 m/s |
| wheel rotation | 166.7 rad/s |
| operating pressure | 101325 Pa |
| pressure outlet | 0 gauge pressure |
| velocity inlet | 55 m/s |
| backflow turbulent intensity | 1 percent |
| backflow turbulent viscosity ratio | 200 |
| | |
| wall condition | vehicle, road |
| symmetry condition | left, right and top boundaries |
| interface conditions | external $\leftrightarrow$ box volumes |
| | box $\leftrightarrow$ boundary layer volumes |